JOURNAL OF GEOPHYSICAL RESEARCH, VOL. 112, C02003, doi:10.1029/2006JC003549, 2007

Effects of wave rollers and bottom stress on wave setup

Alex Apotsos,[1] Britt Raubenheimer,[1] Steve Elgar,[1] R. T. Guza,[2] and Jerry A. Smith[2]

Received 15 February 2006; revised 3 August 2006; accepted 14 August 2006; published 3 February 2007.

[1] Setup, the increase in the mean water level associated with breaking waves, observed between the shoreline and about 6-m water depth on an ocean beach is predicted well by a model that includes the effects of wave rollers and the bottom stress owing to the mean flow. Over the 90-day observational period, the measured and modeled setups are correlated (squared correlation above 0.59) and agree within about 30%. Although rollers may affect setup significantly on beaches with large-amplitude (several meters high) sandbars and may be important in predicting the details of the cross-shore profile of setup, for the data discussed here, rollers have only a small effect on the amount of setup. Conversely, bottom stress (calculated using eddy viscosity and undertow formulations based on the surface dissipation, and assuming that the eddy viscosity is uniform throughout the water column) significantly affects setup predictions. Neglecting bottom stress results in underprediction of the observed setup in all water depths, with maximum underprediction near the shoreline where the observed setup is largest.

Citation: Apotsos, A., B. Raubenheimer, S. Elgar, R. T. Guza, and J. A. Smith (2007), Effects of wave rollers and bottom stress on wave setup, *J. Geophys. Res.*, *112*, C02003, doi:10.1029/2006JC003549.

1. Introduction

[2] Breaking-wave-driven setup is important to coastal flooding and storm damage, with storm-driven increases in sea level having been observed to be more than a meter higher along coastlines exposed to breaking ocean waves than along protected shores. Furthermore, setup is a dominant forcing mechanism for the mean offshore-directed flows in the surf zone (undertow) [*Garcez-Faria et al.*, 2000] that drive sediment offshore during storms [*Thornton et al.*, 1996; *Gallagher et al.*, 1998a].

[3] Assuming alongshore uniform waves and bathymetry and negligible wind stress, the cross-shore pressure gradient associated with the time-averaged wave setup, $\overline{\eta}$, theoretically balances the cross-shore gradient of the time- and depth-averaged cross-shore wave momentum flux (the wave radiation stress, S_{xx}) and the bottom stress, τ_B [*Longuet-Higgins and Stewart*, 1962, 1964; *Stive and Wind*, 1982]

$$\frac{\partial}{\partial x}S_{xx} + \rho g(\overline{\eta} + d)\frac{\partial}{\partial x}\overline{\eta} + \tau_B = 0, \qquad (1)$$

where x is the cross-shore coordinate (positive onshore), d is the time-averaged still water depth, ρ is the water density, and g is the gravitational acceleration.

[4] Field studies of alongshore currents [*Ruessink et al.*, 2001] and laboratory studies of undertow and setup [*Svendsen*, 1984a, 1984b; *Dally and Brown*, 1995] suggest that although linear models of S_{xx} are robust outside the surf zone, nonlinearities in the wave forcing associated with wave rollers (passive regions of circulating water carried onshore by breaking waves) may be important to breaking wave-driven setup [*Reniers and Battjes*, 1997]. Including rollers, the wave radiation stress can be estimated as

$$S_{xx} = E_w\left\{\left[\cos^2\left(\overline{\theta}\right) + 1\right]\frac{c_g}{c} - \frac{1}{2}\right\} + 2E_r\left[\cos^2\left(\overline{\theta}\right)\right], \qquad (2)$$

where $\overline{\theta}$ is the mean wave direction (relative to beach normal), c_g is the group speed, c is the phase speed, E_r is the wave roller energy, and E_w is the wave energy estimated from linear theory as

$$E_w = \frac{1}{8}\rho g H_{rms}^2, \qquad (3)$$

in which H_{rms} is the root-mean-square wave height (defined as $2\sqrt{2}$ times the standard deviation of the sea-surface elevation fluctuations). Rollers may cause a lag between the dissipation of wave energy and the transfer of momentum to the water column, and thus an onshore shift in the location of the maximum wave forcing [*Svendsen*, 1984a].

[5] In the absence of breaking waves, an onshore-directed streaming flow in the viscous bottom boundary layer [*Phillips*, 1966] results in an offshore-directed bottom stress [*Longuet-Higgins*, 2005; *Dean and Bender*, 2006]. However, breaking waves in the surf zone drive an offshore-directed current (undertow) that dominates the onshore streaming [*Haines and Sallenger*, 1994; *Reniers et al.*, 2004], resulting in an onshore-directed bottom stress that increases setup in shallow water.

[6] Laboratory studies suggest that the mean cross-shore momentum balance (equation (1)) is dominated by radiation stress and setup gradients, with negligible contributions

[1]Woods Hole Oceanographic Institution, Woods Hole, Massachusetts, USA.
[2]Scripps Institution of Oceanography, La Jolla, California, USA.

0148-0227/07/2006JC003549$09.00

from bottom stress [*Bowen et al.*, 1968; *Stive and Wind*, 1982; *Dally and Brown*, 1995]. However, bottom stresses and the corresponding forcing of setup may be relatively more important in the field than in the laboratory owing to bedforms, suspended sediments, and alongshore flows.

[7] Field observations in water depths greater than a few meters agree qualitatively with equation (1) when $\tau_B = 0$ [*Battjes and Stive*, 1985; *Lentz and Raubenheimer*, 1999], but setup is underpredicted near and at the shoreline [*Guza and Thornton*, 1981; *Raubenheimer et al.*, 2001]. Here, comparisons of equations (1) and (2) with field observations are used to investigate the importance of rollers and bottom stress to setup on a natural beach.

[8] After roller and bottom stress formulations are discussed (section 2), the observations are described (section 3), and compared with model predictions (section 4). The validity of the bottom stress formulation (section 5) and other processes that may be important to the setup balance (section 6) are discussed, followed by conclusions (section 7).

2. Theory

[9] The wave roller energy E_r is estimated as [*Svendsen*, 1984a, 1984b; *Reniers and Battjes*, 1997]

$$\frac{\partial}{\partial x}\left(2E_r \cos(\overline{\theta})c\right) = -\frac{2gE_r \sin(\beta)}{c} + D_{br}, \tag{4}$$

in which β, the front slope of the wave, is approximated as a constant of 0.1, and the wave dissipation D_{br} is

$$D_{br} = -\frac{\partial}{\partial x}\left(E_w c_g \cos(\overline{\theta})\right). \tag{5}$$

To evaluate effects of alternative roller formulations, three additional models with different forms for E_r (i.e., equation (4)) [*Lippmann et al.*, 1996; J. A. Smith, personal communication] and different values of β [*Tajima*, 2003] were tested. Average setup predictions for the data examined differ by less than 10% among the four models.

[10] The bottom stress, τ_B, is estimated from an eddy viscosity formulation as

$$\tau_B = \rho\nu_e \left.\frac{\partial U}{\partial z}\right|_{z=-d}, \tag{6}$$

where U is the mean depth-dependent cross-shore flow averaged over many surface wave periods, and z is the vertical coordinate with $z = -d$ at the bed. The depth- and time-independent eddy viscosity, ν_e, is estimated as [*Reniers and Battjes*, 1997]

$$\nu_e = \left(\frac{H_{rms}}{14}\right)\left(\frac{c\tau_s}{\rho}\right)^{\frac{1}{3}}, \tag{7}$$

where the constant of 1/14 is based on deepwater wave dissipation [*Terray et al.*, 1996] and observations of Langmuir circulation [*Smith*, 1998]. The results are not sensitive to the eddy viscosity formulation provided that ν_e is similar to values found in prior field studies (see section 5.3).

The surface shear stress, τ_s, assumed to be owing to breaking-wave-induced dissipation, is [*Deigaard*, 1993]

$$\tau_s = -\frac{1}{c}\left\{\frac{\partial}{\partial x}\left[E_w c_g \cos(\overline{\theta})\right] + 2\frac{\partial}{\partial x}\left[E_r c \cos(\overline{\theta})\right]\right\}. \tag{8}$$

Assuming a quadratic variation of the mean flow in the vertical, the undertow is [*Garcez-Faria et al.*, 2000]

$$\frac{\partial^2 U}{\partial (z+d)^2} = a(x), \tag{9}$$

where $a(x)$ is determined from a boundary condition or specified as a forcing term. Integrating equation (9) twice over the water column using a no-slip bottom boundary condition, a surface stress upper boundary condition

$$\tau_s = \rho\nu_e \left.\frac{\partial U}{\partial z}\right|_{z=\eta}, \tag{10}$$

and conservation of mass

$$-(M_w + M_r) = \int_{-d}^{\eta} \rho U dz, \tag{11}$$

where $M_w = E_w/c$ is the mass flux of the wave, and $M_r = 2E_r/c$ is the mass flux of the roller, yields

$$U(z) = a(x)(z+d)^2 + b(x)(z+d), \tag{12}$$

with

$$a(x) = \frac{3}{2h\rho}\left(\frac{\tau_s}{2\nu_e} + \frac{M_w + M_r}{h^2}\right), \tag{13}$$

and

$$b(x) = -\frac{1}{\rho}\left(\frac{\tau_s}{2\nu_e} + \frac{3(M_w + M_r)}{h^2}\right), \tag{14}$$

where h is the total water depth ($h = d + \overline{\eta}$).

[11] Using equations (6) and (12)–(14), the bottom shear stress is

$$\tau_B = \rho\nu_e \left.\frac{\partial U}{\partial z}\right|_{z=-d} = -\left[\frac{1}{2}\tau_s + \frac{3\nu_e(M_w + M_r)}{h^2}\right]. \tag{15}$$

3. Observations

[12] Wave-induced pressures and velocities were measured at 2 Hz for 10752 s (179.2 min) starting every 3 hours using pressure gages and near-bed current meters colocated at 11 cross-shore locations between the shoreline and about 6-m water depth for 90 days during September to November 1997 (SandyDuck experiment) on a barred beach near Duck, NC (Figure 1a). Mean water levels (i.e., setup) were measured at 10 cross-shore locations using pressure gages that were buried to reduce flow noise (*Raubenheimer et al.* [2001], which includes additional description of the setup observa-

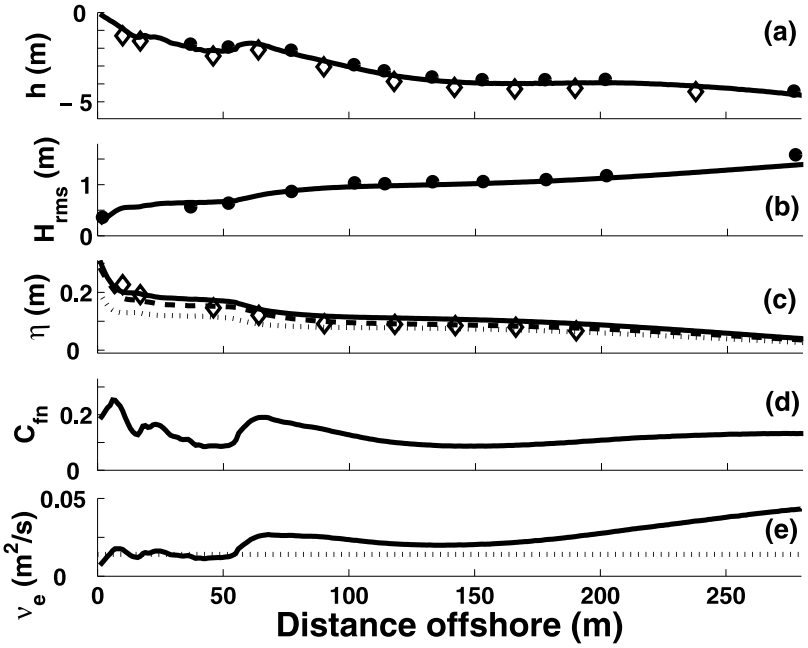

Figure 1. (a) Beach profile (solid curve) relative to still water level, colocated pressure and velocity sensors (circles), and buried pressure sensors (diamonds), (b) observed (circles) and modeled (solid curve) root-mean-square wave heights, (c) observed setup (diamonds) and setup predicted using the full model (equations (1) and (2), solid curve), the model without the roller term (dashed curve), and the model without bottom stress (dotted curve), (d) quadratic friction coefficient, C_{fn}, used to model the bottom stress, and (e) modeled eddy viscosity (e.g., solid curve is equation (7)) versus distance offshore for the 8.5-min data record beginning 13 November, 20:59 hours EST (14 November, 1:59 hours GMT), when the offshore wave height was 2.05 m and the tidal stage was 0.58 m above mean sea level. The horizontal dotted line in Figure 1e is the constant eddy viscosity estimated by *Garcez-Faria et al.* [2000].

tions). The 3-hour-long data records were subdivided into 8.5-min-long sections for processing to ensure stationarity in the presence of tidally induced depth changes. The bathymetry was surveyed approximately every other day from above the shoreline to 8-m water depth along cross-shore transects located about 20 m alongshore (north and south) of the instrumented transect. Additionally, altimeters colocated with the pressure gages and current meters were used to estimate the seafloor location every 3 hours [*Gallagher et al.*, 1998a].

[13] Root-mean-square wave heights ranged from 0.20 to 2.10 m. Mean cross-shore flows ranged from −0.71 to 0.38 m/s (positive onshore) with 95% of the flows between −0.40 and 0.10 m/s. The estimated measurement error of the mean flows is ±0.05 m/s. Setup ranged from −0.03 to 0.50 m with an estimated measurement error of ±0.005 m, increasing to ±0.020 m for the three most shoreward sensors. Centroidal frequencies ranged from 0.08 to 0.21 Hz. Incident wave angles ranged between ±35° relative to beach normal. The nearshore wave field was approximately alongshore uniform and unaffected by the pier, located approximately 340 m south of the instrumented transect, except when the waves approached from the south [*Elgar et al.*, 2001].

[14] The distance between the current meters and the seafloor fluctuated throughout the experiment as the bottom accreted and eroded. The nine offshore sensors usually were in the lower 40% of the water column, whereas the vertical locations of the two sensors nearest the shoreline ranged from near the bottom to near the water surface. For $h > 1$ m, the bathymetry and circulation were approximately alongshore uniform [*Feddersen and Guza*, 2003], and observations of rip currents were infrequent. However, for $h < 1$ m, comparisons of the surveys 20 m north and south of the instrumented transect suggest errors in the estimated distance between the sensor and the seafloor may be as large as 25% of the water depth. Additionally, in the shallowest depths the seafloor location changed by as much as 50% of h between consecutive profiles.

[15] To force the setup model, wave characteristics were estimated at 1-m cross-shore spacing. Wave directions were estimated from Snell's Law and the measurements in about 6-m water depth, c_g and c were calculated from the measured bathymetry and centroidal frequencies, and wave heights were determined from one of six one-dimensional wave transformation models.

[16] Three wave transformation models [*Thornton and Guza*, 1983; *Church and Thornton*, 1993; *Lippmann et al.*, 1996] with a free parameter, γ, were fit to the data over a physically realistic range (i.e., $0.1 < \gamma < 1$). The root-mean-square (rms) percent error between the observations and predictions was minimized for each wave model for each data record. Three wave transformation models [*Baldock et al.*, 1998; *Tajima*, 2003; *Ruessink et al.*, 2003] without free parameters also were used to predict the wave heights, and rms errors were calculated for each data record. The wave model with the smallest cross-shore rms error was selected for each data record. The models of *Thornton and Guza* [1983], *Lippmann et al.* [1996], *Church and Thornton*

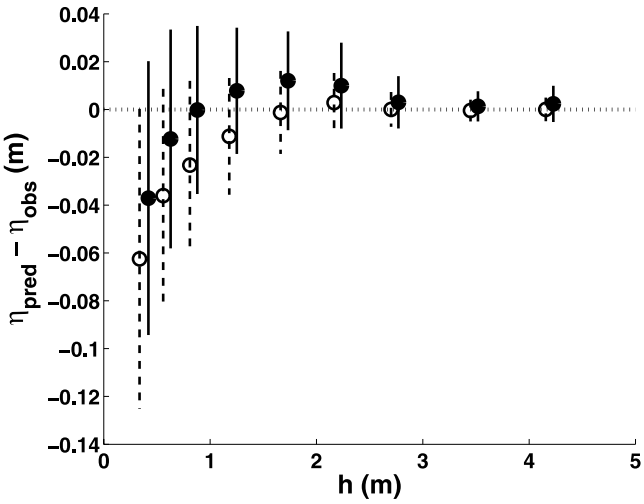

Figure 2. Mean errors and standard deviations for the full setup model (solid circles and lines, respectively) and for the model without either rollers or bottom stress (open circles and dashed lines, respectively) versus depth. Dashed lines and open circles are plotted offset by 0.1 m in h for clarity.

[1993], *Baldock et al.* [1998], *Ruessink et al.* [2003], and *Tajima* [2003] were used for 48%, 23%, 21%, 5%, 2%, and 1% of the data records, respectively. The resulting modeled cross-shore wave heights are typically within 13% of the observations (e.g., Figure 1b) and have a mean error of ≈6%.

4. Comparison of Observed and Modeled Setup

4.1. Full Model

[17] The setup model predictions are consistent with the observations (Figures 1c (compare solid curve with diamonds), 2, and 3). The model overpredicts setup by about 20% for $h > 1$ m, and underpredicts setup by about 30% for $h < 1$ m. In water depth ranges $3.0 < h < 6.0$ m, $1.0 < h < 3.0$ m, and $0.3 < h < 1.0$ m, the best fit slopes between the model predictions and the observations are 1.22, 1.11, and 0.68, respectively (Table 1), where values less than 1 indicate underprediction. Setup and setdown in the deepest water (Figure 3, right-hand panels) often were smaller than the measurement error, and thus the slope of the linear regression may be inaccurate. Furthermore, the slope is biased by the few cases with large waves and significant observed setup. In all depths, squared correlations (r^2) between model predictions and observations are greater than about 0.59, mean errors are less than 0.012 m, and rms errors are less than 0.050 m (Table 1).

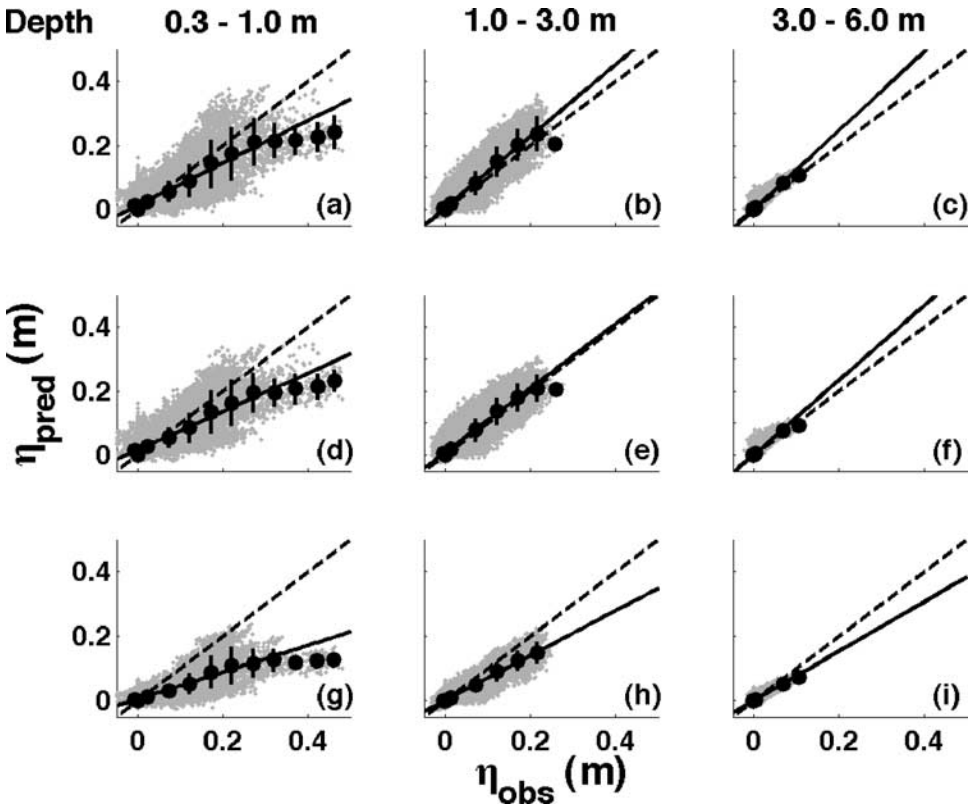

Figure 3. Predicted versus observed setup for the entire 90-day data set for (a–c) the full model, (d–f) the model without rollers, and (g–i) the model without bottom stress, for water depths $0.3 < h < 1.0$ (Figures 3a, 3d, and 3g), $1.0 < h < 3.0$ (Figures 3b, 3e, and 3h), and $3.0 < h < 6.0$ m (Figures 3c, 3f, and 3i). Light grey clouds are unbinned 8.5-min values. Solid circles and vertical hashes are the means (0.05-m-wide bins) and standard deviations, respectively. The solid and dashed black lines are the least squares fits to the unbinned values and the perfect fits (i.e., 1 to 1 comparison), respectively.

Table 1. Squared Correlation Coefficients, Best Fit Slopes, Intercepts, Root-Mean-Squared Errors, and Mean Errors for Water Depths $0.3 < h < 1.0$, $1.0 < h < 3.0$, and $3.0 < h < 6.0$ m

Depths, m	r^2	Slope	Intercept, m	RMS Error, m	Mean Error, m
			Full Model		
0.3–1	0.59	0.68	0.010	0.048	−0.012
1–3	0.83	1.11	0.006	0.023	0.009
3–6	0.77	1.22	0.001	0.007	0.002
			Model Without Roller		
0.3–1	0.59	0.61	0.014	0.048	−0.012
1–3	0.78	1.00	0.009	0.023	0.009
3–6	0.73	1.16	0.002	0.007	0.002
			Model Without Bottom Stress		
0.3–1	0.57	0.42	0.002	0.061	−0.037
1–3	0.85	0.69	0.001	0.018	−0.006
3–6	0.80	0.76	0.000	0.004	−0.001
			Model Without Roller or Bottom Stress[a]		
0.3–1	0.58	0.38	0.007	0.061	−0.036
1–3	0.79	0.62	0.004	0.020	−0.004
3–6	0.75	0.72	0.000	0.005	−0.000

[a]This model corrects an error in the work of *Raubenheimer et al.* [2001].

4.2. Effects of Wave Rollers

[18] Excluding wave rollers (i.e., $E_r = 0$ in equation (2)) does not affect the setup predictions significantly (e.g., Figure 1c; compare the dashed curve with the solid curve). The mean and rms errors between model predictions and observations are the same as those for E_r estimated from equation (4), while the best-fit slopes decrease by about 10% (Table 1). Although the roller has little effect on the magnitude of the nearshore setup, including the roller shifts the transition from setdown to setup onshore by an average of 6 m relative to model predictions without rollers. Therefore accurate modeling of the roller may be important in predicting the cross-shore profile of setup.

[19] Increasing (decreasing) $\sin(\beta)$ shifts the setup forcing offshore (onshore), resulting in increased (decreased) setup offshore of the sandbar (not shown). However, onshore of the bar, momentum may be advected into the deeper water of the trough, resulting in decreased setup. Thus, depending on the magnitude of $\sin(\beta)$, the height of the bar, and the depth of the trough, setup onshore of the trough may be increased or decreased by increasing $\sin(\beta)$. Average setup predictions at SandyDuck differ by less than 10% for $\sin(\beta) =$ 0.05, 0.10, or 0.20.

4.3. Bottom Stress

[20] Excluding bottom stress in the momentum balance (i.e., $\tau_B = 0$ in equation (1)) significantly degrades setup predictions in shallow water (e.g., Figure 1c, compare the dotted curve with the solid curve). For $0.3 < h < 1.0$ m, the mean setup error is 3 times larger when bottom stress is neglected than when it is included (Table 1). Although changes in the squared correlations between predictions and observations are small, neglecting bottom stress results in a 38% decrease (i.e., underprediction increases) of the best fit slopes and a 27% increase in rms errors (Table 1). However, excluding bottom stress causes the transition from setdown to setup to occur farther onshore, eliminating the overprediction of setup observed for $h > 1$ m (e.g., for $1 < h <$ 3 m, the mean error decreases by 33% and the best fit slope decreases from 1.11 to 0.69). The overprediction of setup when bottom stress is included may result from a poor representation of stress in the deeper water offshore of the bar. Also, the undertow and eddy viscosity models are not valid outside the surf zone, and thus equation (15) may be inaccurate in this region. Including the roller partly balances the offshore shift of the transition from setdown to setup that results from including bottom stress.

5. Discussion

5.1. Observational Errors

[21] Scatter in the 8.5-min setup observations may be partly owing to the presence of "surfbeat" or infragravity waves (periods > 30 s). However, results using 34-min and 1-hour averages suggest this scatter does not affect the trends and biases in the model-data comparisons presented here. Setup predictions based on bathymetric profiles generated from a cubic spline of the 3-hour altimeter measurements are similar to those based on the surveyed bathymetry, suggesting that bathymetric errors are not important to the results. The accuracy of parametric wave models decreases over bar troughs [*Ruessink et al.*, 2003] and in shallow water, which may cause errors in the setup predictions. However, interpolating the observed waves with a cubic spline instead of with a wave transformation model has little effect on the results. Excluding records with southerly swell (offshore waves arriving more than 15° south of shore normal) that might be affected by the pier has a negligible effect on the results.

5.2. Bottom Stresses

[22] The present bottom stress estimates are compared with estimates based on a Darcy-Weisbach equation. The friction coefficients, C_{fn}, needed to obtain bottom stresses similar to those calculated by equation (15) are estimated from a simplified quadratic friction model [*Dally and Brown*, 1995]

$$C_{fn} = \frac{\tau_B}{|u_{orb}|U_m\rho}, \tag{16}$$

where $|u_{orb}|$ is the maximum wave-orbital velocity calculated from wave heights and water depths using linear, shallow water wave theory, and a Rayleigh wave height distribution [*Thornton and Guza*, 1986]

$$|u_{orb}| = \frac{1}{2}\left(\frac{g}{h}\right)^{1/2}\left[\frac{\sqrt{\pi}}{2}H_{rms}\right]\left(\frac{2}{\pi}\right). \quad (17)$$

The mean return current, U_m, is estimated as

$$U_m = \frac{M_w + M_r}{\rho h}. \quad (18)$$

For the 8.5-min data record shown in Figure 1, $0.06 < C_{fn} < 0.26$ (Figure 1d). For the full 3-month data set, the mean value of C_{fn} in the surf zone is 0.18, with a range of $0 < C_{fn} < 0.53$. Note that C_{fn} can approach 0 in the bar trough where breaking ceases and $\tau_B \approx 0$.

[23] A Darcy-Weisbach equation with a Manning coefficient can be used to estimate C_{fn} [*Dally and Brown*, 1995]. Using a Manning coefficient of 0.030 s/m$^{1/3}$ [*Arcement and Schneider*, 1990], a value approximately in the middle of the range for slightly rough, natural sandy channels (0.026–0.035 s/m$^{1/3}$), C_{fn} is estimated as 0.017, 0.011, and 0.008 for 0.3-, 1.0-, and 3.0-m water depths, respectively. While these values are approximately an order of magnitude smaller than found from equation (16), the Darcy-Weisbach equation does not account for the turbulence generated by breaking waves, bedforms, or wave-current interactions, and thus C_{fn} likely is biased low. Observations [*Carstens et al.*, 1969] and theoretical calculations [*Longuet-Higgins*, 1981] have shown the drag coefficient can be larger by an order of magnitude or more over rippled sand beds.

[24] To compare the present bottom stress estimates with prior estimates based on cross- and alongshore momentum balances, the friction coefficients, C_{fn2}, needed to obtain bottom stresses similar to those calculated by equation (15) are estimated as

$$C_{fn2} = \frac{\tau_B}{\langle|\vec{u}|u\rangle\rho}, \quad (19)$$

where $|\vec{u}|$ is the magnitude of the total instantaneous velocity, u is the instantaneous velocity in the cross-shore direction, and $\langle\rangle$ is a time average. Equation (15) always predicts an onshore-directed bottom stress, and thus a time-averaged onshore-directed flow results in an unrealistic negative C_{fn2} in (19). These negative coefficients, which account for 32% of the surf zone estimates and 50% of the estimates seaward of the surf zone, may be caused by inaccuracies in the flow measurements for small velocities, local nonuniformities in the bathymetry, or velocity measurements in the upper water column where onshore flow is expected. On the basis of a linear regression between the modeled τ_B (e.g., equation (15)) and the measured $\langle|\vec{u}|u\rangle$ at the location of each sensor, and neglecting negative values of C_{fn2} [e.g., *Feddersen et al.*, 1998], the squared correlations between τ_B and $\langle|\vec{u}|u\rangle$ inside and seaward of the surf zone are $r^2 = 0.19$ and $r^2 = 0.51$, respectively (Figure 4). Similar to previous results [*Feddersen et al.*, 1998], the best fit C_{fn2} is higher inside the surf zone (0.028) than seaward of the surf zone (0.018), although the friction coefficients estimated here are larger than previous estimates (0.007–0.020 [*Longuet-Higgins*, 1970]; 0.015 [*Raubenheimer et al.*, 1995]; 0.007–0.015 [*Reniers and Battjes*, 1997]; 0.001–0.012 [*Garcez-Faria et al.*, 1998]; 0.002–0.003 [*Feddersen et al.*, 1998]). The orientation of bedforms, which frequently are observed on this beach [*Gallagher et al.*, 1998b], may influence cross-shore and alongshore flows differently [*Barrantes and Madsen*, 2000]. Consequently, significantly smaller drag coefficients may be estimated for alongshore flows [i.e., *Garcez-Faria et al.*, 1998; *Feddersen et al.*, 1998] than for cross-shore flows.

5.3. Eddy Viscosity

[25] The eddy viscosity is assumed to be proportional to turbulence intensity [*Garcez-Faria et al.*, 2000], and varies in the cross-shore as waves change across the surf zone (Figure 1e). The range of ν_e over the entire 3 month period, $0 < \nu_e < 0.056$ m^2/s, is consistent with prior undertow studies [*Haines and Sallenger*, 1994; *Garcez-Faria et al.*, 2000].

[26] The modeled bottom stress and setup are only weakly sensitive to the cross-shore dependence of ν_e and to 50% changes in its magnitude, because increasing ν_e decreases the shear of the mean flow near the bed (e.g., equation (6)). Reducing ν_e by 50% or using a constant ν_e of 0.014 m^2/s [*Garcez-Faria et al.*, 2000] has a much smaller effect on the modeled setup than excluding the bottom stress (a 9% decrease compared with a 38% decrease in the best-fit slopes, and a 33% increase compared with a 208% increase in the mean errors, respectively for $0.3 < h < 1.0$ m).

[27] If wave-breaking induced turbulence reaches the bed [e.g., *Cox and Kobayashi*, 2000], a vertically constant eddy viscosity (such as that used here) may be appropriate. However, if the water column is not well mixed, the eddy viscosity may be significantly smaller in the bottom boundary layer than in the mid-water-column [e.g., *Svendsen et al.*, 1987; *Reniers et al.*, 2004], greatly reducing the effect of the bottom stress on setup. For example, the effect of the bottom stress is near zero using the bottom boundary layer eddy viscosity proposed by *Reniers et al.* [2004]. In deep water, the penetration depth of surface turbulence is proportional to the wave height, with little reduction in turbulence strength to a depth below the surface of $0.71H_{rms}$ [*Terray et al.*, 1996]. In shallow water, surface-generated turbulence can penetrate to the bottom boundary layer, increasing the local bottom shear stress [*Fredsøe et al.*, 2003]. On the basis of these results and the observation that at breaking $H_{rms}/h \approx 0.4$ and increases toward the shoreline [*Raubenheimer et al.*, 1996], breaking-wave-generated turbulence may be reaching the bottom inside the surf zone.

[28] However, in the outer surf zone, surface-generated turbulence does not penetrate to the bed [*Trowbridge and Elgar*, 2001]. Similarly, C_{fn2} (an indicator of bottom stress) for alongshore currents is inversely proportional to water depth [*Feddersen and Trowbridge*, 2005], which may be a proxy for the strength of wave breaking. Thus it is possible that surface generated turbulence may reach the bottom only during significant wave breaking or in the inner to middle surf zone. If bottom stress is included in the model only during intense dissipation (defined here to be when wave energy is decreasing 3% per meter in the cross-shore), setup is predicted more accurately for $h > 1$ m (for $1.0 < h < 3.0$ m, the mean error is -0.002 m and the best fit slope is 0.84, for

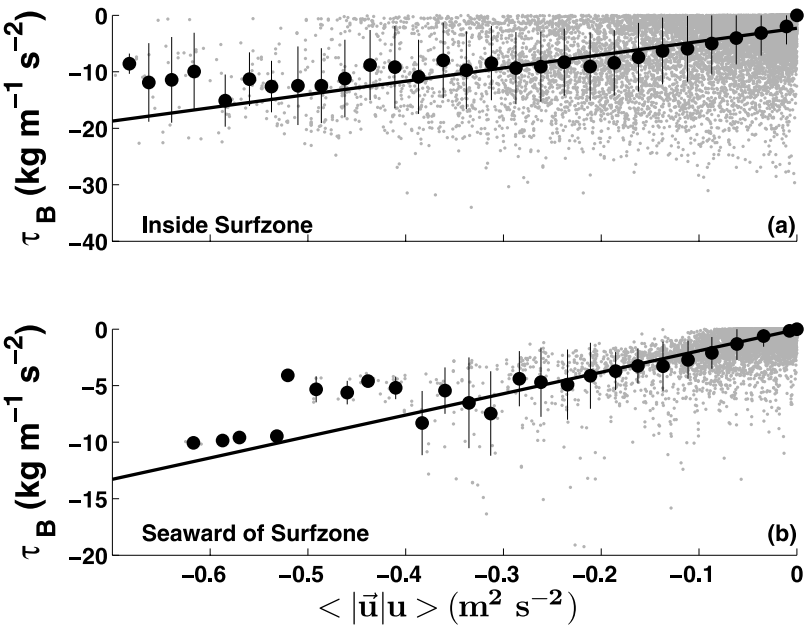

Figure 4. Bottom stress, τ_B, from equation (15) versus $\langle|\overrightarrow{u}|u\rangle$ for (a) the surf zone and (b) seaward of the surf zone. Light grey dots are unbinned 8.5-min values. Solid circles and vertical hashes are the means (0.025-m^2/s^2 - wide bins) and standard deviations, respectively. The solid lines are the least squares fits to the unbinned values. The results do not change if 3-hour averages are used instead of the 8.5-min averages.

$3.0 < h < 6.0$ m the mean error is -0.001 m and the best fit slope is 0.80, compare with the values in Table 1), but less accurately for $h < 1$ m (for $0.3 < h < 1.0$ the mean error is -0.024 m and best fit slope is 0.56).

5.4. Mean Flows

[29] Using only flows greater than the sensor accuracy (i.e., magnitude greater than 0.05 m/s), it is found that modeled mean flows at the elevations of the current meters are within a factor of 3 of the observed flows (Figure 5) and on average the model underpredicts the observed undertow. Differences between modeled and observed mean flows ($r^2 < 0.2$) may result from inaccuracies in the bottom locations, and thus in errors in estimates of the elevation of the sensor above the bed (see Appendix A). The uncertainty in the total water depth and in the elevation of the current meters above the bed precludes using a single current meter to test the undertow model predictions.

5.5. Effects of a Large Offshore Bar

[30] The presence of a large-amplitude sandbar increases the importance of rollers to setup. Numerical simulations over bathymetry observed near Egmond, The Netherlands, on 18 October 1998 when a large bar (height > 3 m) was present [*Ruessink et al.*, 2001] show that the change in setup owing to neglecting the roller relative to the setup predicted with the full model was often 15% when $H_{rms} > 1$ m, and in some cases exceeded 22% (Figure 6a, compare solid with dashed curve). However, for small waves or high tidal states (when the bar was located farther offshore and in deeper water), the effect of rollers on the setup is similar to that found at SandyDuck. Furthermore, the effect of the roller for eight days during SandyDuck when a bar (height > 0.50 m and width > 20 m) was present, as well as for numerical simulations using the barred (height $\approx$ 1 m and width $\approx$ 80 m) bathymetry from 26 October 1994 (Duck94 experiment [*Elgar et al.*, 1997]) is similar to the effect for all bathymetries at SandyDuck. The numerical simulations over the Egmond and Duck94 bathymetry indicate that the effect of bottom stress on setup also is significant on beaches with large offshore bars (Figure 6a, compare solid with dotted curve).

6. Other Terms

[31] It has been suggested that broad wave directional spreads, wave skewness, large wind stresses, convective accelerations of the current, wave-generated near-bottom flow asymmetry, onshore-directed streaming flow, and alongshore inhomogeneous bathymetry or wave conditions could affect setup predictions in shallow water. Incorporating terms that correct the radiation stress estimates for the observed directional spreads [*Feddersen*, 2004] and for wave skewness [*Johnson and Kobayashi*, 1998] has a negligible effect on the setup predictions. Wind speeds and convective accelerations of the current (estimated following *Dally and Brown* [1995]) are small, and the estimated setup forcing owing to these terms is negligible. Neglecting wave-generated flow asymmetry and onshore-directed streaming flow [e.g., *Longuet-Higgins*, 2005; *Dean and Bender*, 2006] may explain partly the overprediction of setup in the shoaling and outer surf zone regions where the undertow is relatively small. The two-dimensional setup forcing term $\left(\frac{\partial S_{xy}}{\partial y}\right)$ was estimated from differences between S_{xy} calculated using the wave models and Snell's Law along two cross-shore transects approximately 20 m north and

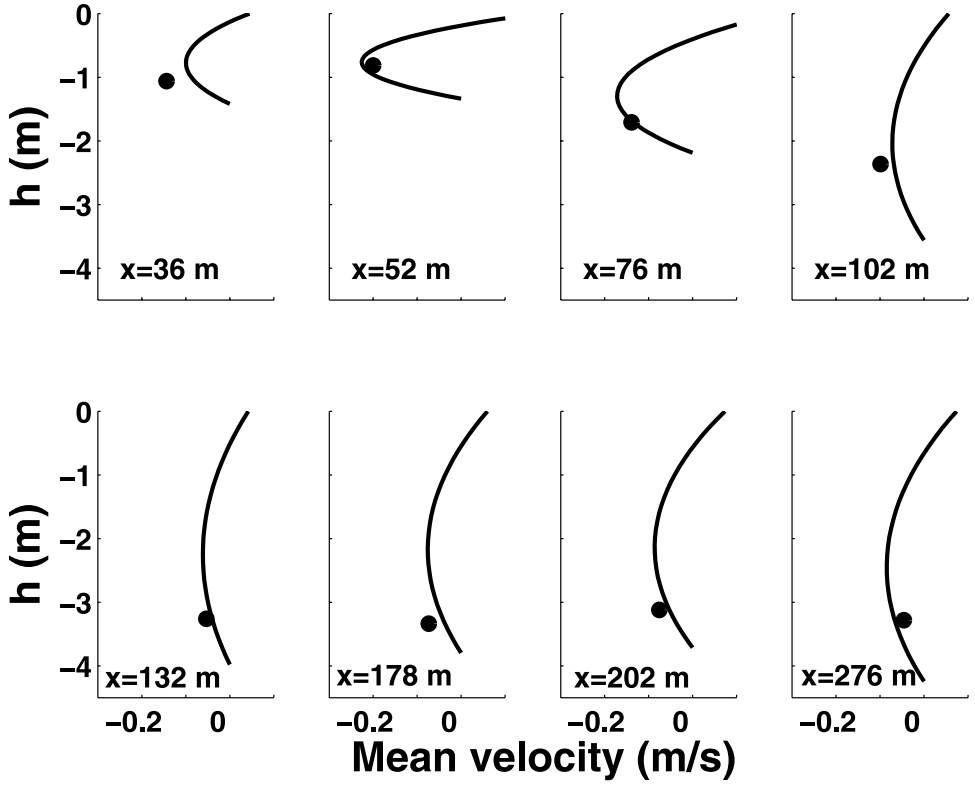

Figure 5. Observed (circles) and predicted (curves) mean cross-shore flows (undertow) as a function of water depth for the 8.5-min data record beginning 27 September, 19:51 hours EST (23:51 hours GMT).

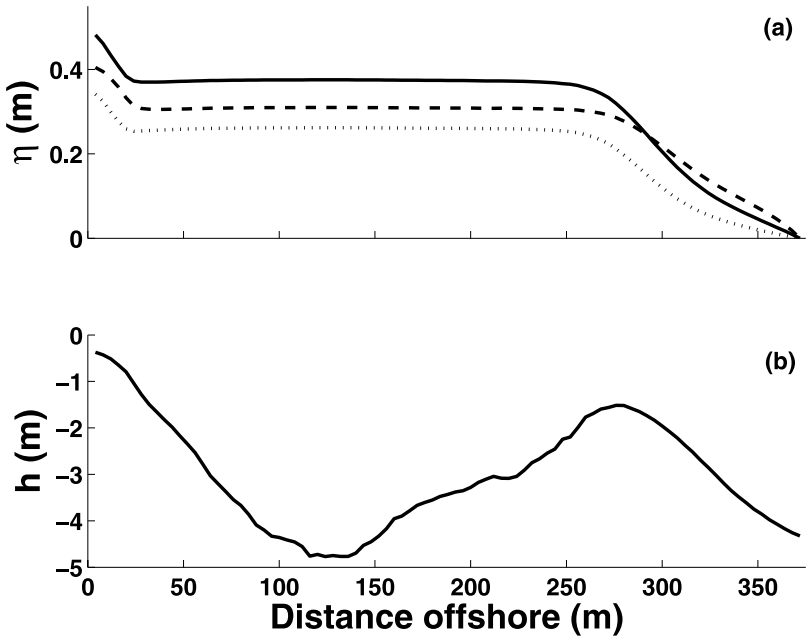

Figure 6. (a) Setup simulated using the full model (equations (1) and (2), solid curve), the model without the roller term (dashed curve), and the model without the bottom stress term (dotted curve) for (b) the barred beach profile near Egmond, The Netherlands, on 18 October 1998 relative to still water level versus the distance offshore. For this simulation the offshore wave height was 2.1 m, and the still water (tidal) level was −1.7 m relative to mean sea level.

south of the instrumented transect. For $h < 1$ m, on average $\frac{\partial S_{xy}}{\partial y}$ is less than 1% of the cross-shore term ($\frac{\partial S_{xx}}{\partial x}$) and exceeds $\frac{\partial S_{xx}}{\partial x}$ by 5% less than 2% of the time, and thus does not affect the setup model results presented here.

7. Conclusions

[32] Field observations of wave setup were compared with model predictions that include the effects of wave rollers and bottom stress. The modeled and observed setup are correlated (r^2 above 0.59), and agree within about 30%. Rollers typically have only a small effect on the magnitude of setup in this study, but may be important to the details of the cross-shore setup profile and to setup on beaches with larger-amplitude sandbars. Bottom stress significantly affects the setup predictions. For $0.3 < h < 1.0$ m, excluding bottom stress increases the mean error in setup predictions by a factor of about 3. Although excluding bottom stress does not change the correlation between model predictions and observations, the best-fit slope decreases by 38% (i.e., underprediction increases) and the rms error increases by about 27%. Estimated eddy viscosities used to calculate the bottom stress are similar to values found in previous field experiments. However, the estimated bottom stresses and friction coefficients are larger than expected from prior laboratory studies and from field studies of alongshore flows. The high friction coefficients may be related to the assumption of a vertically constant eddy viscosity, as would be appropriate if breaking-wave-generated turbulence penetrates to the bed. Thus the model presented here may be valid only in the inner and middle surf zone where surface-generated turbulence reaches the seafloor.

Appendix A: Undertow Estimates

[33] Underprediction of the undertow may be partly owing to an overestimate of the eddy viscosity, ν_e. Reducing ν_e gives a more parabolic undertow profile and larger mean flows at most sensor elevations. Alternatively, the assumption of a parabolic vertical profile for the undertow (e.g., equation (9)) may be invalid in the trough region [*Garcez-Faria et al.*, 2000; *Reniers et al.*, 2004], resulting in undertow prediction errors. Seaward of the surf zone the possible presence of near-bottom onshore streaming flow and the prediction of a nonzero eddy viscosity owing to a small dissipation calculated from the wave models also may produce errors in flow predictions. Deviations between the modeled and observed undertow also may be owing to inaccurate measurements of the bottom profile, leading to incorrect elevations of the sensors above the bed.

[34] When the undertow results are restricted to cases for which the root-mean-square error between the local altimeter depth measurements and the bathymetry surveyed 20 m north and south of the instrumented transect is less than 0.1 m and H_{rms} offshore is greater than 0.6 m, and if the undertow prediction elevations are allowed to vary from the sensor elevation by up to ±0.2 m (the average difference in elevation for consecutive and bracketing profiles), the agreement between the modeled and observed mean flows is greatly improved, with most of the improvement owing to the variation in the sensor elevation. However, the modeled undertow can change significantly over a vertical range of 0.4 m. On the basis of the sensitivity of the undertow predictions to the sensor elevations and the water depth, the single vertical measurements of undertow used here are insufficient to test undertow profile models.

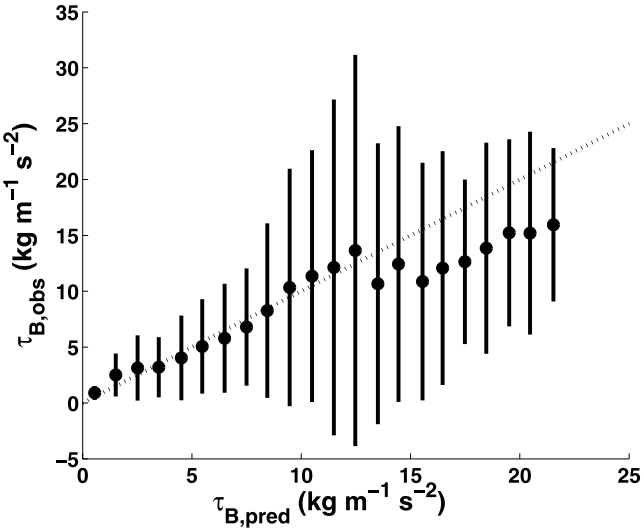

Figure A1. Means (circles, 1-kg m^{-1} s^{-2}-wide bins) and standard deviations (solid lines) of $\tau_{B,obs}$ calculated from the observed undertow assuming a linear variation with depth and a no-slip bottom boundary condition versus $\tau_{B,pred}$ modeled using equation (15). The dotted line is perfect agreement.

[35] The effect of inaccurately modeled mean flows on the bottom stress estimates is investigated in two ways. First, several undertow models [*Haines and Sallenger*, 1994; *Garcez-Faria et al.*, 2000; *Reniers et al.*, 2004] were used to estimate the near-bottom velocity gradients. As long as the models include a no-slip bottom boundary condition (e.g., *Garcez-Faria et al.* [2000] was modified to include one) and a depth-averaged eddy viscosity representative of the entire water column is used in equation (6), the choice of undertow model does not alter the conclusion that bottom stress significantly affects setup. Second, modeled bottom stresses (e.g., equation (15)) were compared with estimates, $\tau_{B,obs}$, using the observed mean flows, a no-slip bottom boundary condition, and by assuming a linear variation of the mean flow between the bed and the measurement location. Prior field studies show that the undertow reaches a maximum below the middle of the water column [*Reniers et al.*, 2004], and only flow measurements in the lower 40% of the water column are used to ensure that flows decrease monotonically toward the bed. The nine offshore sensors were in the bottom 40% of the water column 96% of the time, whereas the two sensors nearest the shoreline were in the bottom 40% of the water column 34% of the time. The unbinned 8.5-min values of $\tau_{B,obs}$ are poorly correlated ($r^2 = 0.21$, not shown) with equation (15). On the basis of the approximations made in estimating $\tau_{B,obs}$, the uncertainty in the sensor elevations above the seafloor, and the poor spatial resolution of the current meters, extrapolating these point observations to comment on the individual model runs is

not useful. However, the average estimates of bottom stress from the modeled and observed flows agree well (Figure A1, $r^2 = 0.93$, rms error = 2.49 kg/ms^2), suggesting that, on average, the undertow formulation does not bias the bottom stress estimates significantly. The large cross-shore separation between current meters precludes driving the setup model with stresses estimated from the observed flows.

[36] **Acknowledgments.** Funding was provided by the Office of Naval Research, the National Science Foundation, and the Army Research Office. Staff from the U.S. Army Corps of Engineering Field Research Facility and the Center for Coastal Studies provided excellent logistical support during data collection. The reviewers are thanked for their insightful suggestions and comments.

References

Arcement, G. J., and V. R. Schneider (1990), Guide for selecting Manning's roughness coefficients for natural channels and flood plains, *Water Supply Pap. 2339*, U.S. Geol. Surv., Reston, Va.

Baldock, T. E., P. Holmes, S. Bunker, and P. Van Weert (1998), Cross-shore hydrodynamics within an unsaturated surf zone, *Coastal Eng.*, *34*, 173–196.

Barrantes, A. I., and O. S. Madsen (2000), Near-bottom flow and resistance for currents obliquely incident to two-dimensional roughness elements, *J. Geophys. Res.*, *105*, 26,253–26,264.

Battjes, J. A., and M. J. F. Stive (1985), Calibration and verification of a dissipation model for random breaking waves, *J. Geophys. Res.*, *90*, 9159–9167.

Bowen, A. J., D. L. Inman, and V. P. Simmons (1968), Wave 'set-down' and set-up, *J. Geophys. Res.*, *73*, 2569–2577.

Carstens, M. R., F. M. Nielson, and H. D. Altinbilek (1969), Bed forms generated in the laboratory under oscillatory flow, *Tech. Mem. 28*, Coastal Eng. Res. Cent., Fort Belvoir, Va.

Church, J. C., and E. B. Thornton (1993), Effects of breaking wave induced turbulence within a longshore current model, *Coastal Eng.*, *20*, 1–28.

Cox, D. T., and N. Kobayashi (2000), Identification of intense, intermittent coherent motions under shoaling and breaking waves, *J. Geophys. Res.*, *105*, 14,223–14,236.

Dally, W. R., and C. A. Brown (1995), A modeling investigation of the breaking wave roller with application to cross-shore currents, *J. Geophys. Res.*, *100*, 24,873–24,883.

Dean, R. G., and C. J. Bender (2006), Static wave setup with emphasis on damping effects by vegetation and bottom stress, *Coastal Eng.*, *53*, 149–156.

Deigaard, R. (1993), A note on the three-dimensional shear stress distribution in a surf zone, *Coastal Eng.*, *20*, 157–171.

Elgar, S., R. T. Guza, B. Raubenheimer, T. H. C. Herbers, and E. Gallagher (1997), Spectral evolution of shoaling and breaking waves on a barred beach, *J. Geophys. Res.*, *102*, 15,797–15,805.

Elgar, S., R. T. Guza, W. C. O'Reilly, B. Raubenheimer, and T. H. C. Herbers (2001), Wave energy and direction observed near a pier, *J. Waterw. Port Coastal Ocean Eng.*, *127*(1), 2–6.

Feddersen, F. (2004), Effect of wave directional spread on the radiation stress: Comparing theory and observations, *Coastal Eng.*, *51*, 473–481.

Feddersen, F., and R. T. Guza (2003), Observations of nearshore circulation: Alongshore uniformity, *J. Geophys. Res.*, *108*(C1), 3006, doi:10.1029/2001JC001293.

Feddersen, F., and J. H. Trowbridge (2005), The effect of wave breaking on surfzone turbulence and alongshore currents: A modeling study, *J. Phys. Oceanogr.*, *35*, 2187–2203.

Feddersen, F., R. T. Guza, S. Elgar, and T. H. C. Herbers (1998), Alongshore momentum balances in the nearshore, *J. Geophys. Res.*, *103*, 15,667–15,676.

Fredsøe, J., B. M. Sumer, A. Kozakiewicz, L. H. C. Chua, and R. Deigaard (2003), Effect of externally generated turbulence on wave boundary layer, *Coastal Eng.*, *49*, 155–183.

Gallagher, E. L., S. Elgar, and R. T. Guza (1998a), Observations of sand bar evolution on a natural beach, *J. Geophys. Res.*, *103*, 3203–3215.

Gallagher, E. L., S. Elgar, and E. B. Thornton (1998b), Megaripple migration in a natural surfzone, *Nature*, *394*, 165–168.

Garcez-Faria, A. F., E. B. Thornton, T. P. Stanton, C. V. Soares, and T. C. Lippmann (1998), Vertical profiles of longshore currents and related bed shear stress and bottom roughness, *J. Geophys. Res.*, *103*, 3217–3232.

Garcez-Faria, A. F., E. B. Thornton, T. C. Lippmann, and T. P. Stanton (2000), Undertow over a barred beach, *J. Geophys. Res.*, *105*, 16,999–17,010.

Guza, R. T., and E. B. Thornton (1981), Wave set-up on a natural beach, *J. Geophys. Res.*, *86*, 4133–4137.

Haines, J. W., and A. H. Sallenger Jr. (1994), Vertical structure of mean cross-shore currents across a barred surf zone, *J. Geophys. Res.*, *99*, 14,223–14,242.

Johnson, B. D., and N. Kobayashi (1998), Nonlinear time-averaged model in surf and swash zones, paper presented at International Conference on Coastal Engineering, Am. Soc. of Civ. Eng., Copenhagen.

Lentz, S., and B. Raubenheimer (1999), Field observations of wave setup, *J. Geophys. Res.*, *104*, 25,867–25,875.

Lippmann, T. C., A. H. Brookins, and E. B. Thornton (1996), Wave energy transformation on natural profiles, *Coastal Eng.*, *27*, 1–20.

Longuet-Higgins, M. S. (1970), Longshore currents generated by obliquely incident sea waves, *J. Geophys. Res.*, *75*, 6778–6789.

Longuet-Higgins, M. S. (1981), Oscillating flow over steep sand ripples, *J. Fluid Mech.*, *107*, 1–35.

Longuet-Higgins, M. S. (2005), On wave set-up in shoaling water with a rough sea bed, *J. Fluid Mech.*, *527*, 217–234.

Longuet-Higgins, M. S., and R. W. Stewart (1962), Radiation stress and mass transport in gravity waves, with application to 'surf-beats', *J. Fluid Mech.*, *13*, 481–504.

Longuet-Higgins, M. S., and R. W. Stewart (1964), Radiation stresses in water waves: A physical discussion with application, *Deep Sea Res.*, *11*, 529–562.

Phillips, O. M. (1966), *The Dynamics of the Upper Ocean*, Cambridge Univ. Press, New York.

Raubenheimer, B., R. T. Guza, S. Elgar, and N. Kobayashi (1995), Swash on a gently sloping beach, *J. Geophys. Res.*, *100*, 8751–8760.

Raubenheimer, B., R. T. Guza, and S. Elgar (1996), Wave transformation across the inner surf zone, *J. Geophys. Res.*, *101*, 25,589–25,597.

Raubenheimer, B., R. T. Guza, and S. Elgar (2001), Field observations of wave-driven setdown and setup, *J. Geophys. Res.*, *106*, 4629–4638.

Reniers, A. J., and J. A. Battjes (1997), A laboratory study of longshore currents over barred and non-barred beaches, *Coastal Eng.*, *30*, 1–22.

Reniers, A. J., E. B. Thornton, T. P. Stanton, and J. A. Roelvink (2004), Vertical flow structure during Sandy Duck: Observations and modeling, *Coastal Eng.*, *51*, 237–260.

Ruessink, B. G., J. R. Miles, F. Feddersen, R. T. Guza, and S. Elgar (2001), Modeling the alongshore current on barred beaches, *J. Geophys. Res.*, *106*, 22,451–22,463.

Ruessink, B. G., D. J. R. Walstra, and H. N. Southgate (2003), Calibration and verification of a parametric wave model on barred beaches, *Coastal Eng.*, *48*, 139–149.

Smith, J. A. (1998), Evolution of Langmuir circulation during a storm, *J. Geophys. Res.*, *103*, 12,649–12,668.

Stive, M. J. F., and H. G. Wind (1982), A study of radiation stress and set-up in the nearshore region, *Coastal Eng.*, *6*, 1–25.

Svendsen, I. A. (1984a), Wave heights and set-up in a surf zone, *Coastal Eng.*, *8*, 303–329.

Svendsen, I. A. (1984b), Mass flux and undertow in a surf zone, *Coastal Eng.*, *8*, 347–365.

Svendsen, I. A., H. A. Schäffer, and J. Buhr Hansen (1987), The interaction between the undertow and the boundary layer flow on a beach, *J. Geophys. Res.*, *92*, 11,845–11,856.

Tajima, Y. (2003), Surf-zone hydrodynamics, Ph.D. thesis, Mass. Inst. of Technol., Cambridge, Mass.

Terray, E. A., M. A. Donelan, Y. C. Agrawal, W. M. Drennan, K. K. Kahma, A. J. Williams III, P. A. Hwang, and S. A. Kitaigorodski (1996), Estimates of kinetic energy dissipation under breaking waves, *J. Phys. Oceanogr.*, *26*, 792–807.

Thornton, E. B., and R. T. Guza (1983), Transformation of wave height distribution, *J. Geophys. Res.*, *88*, 5925–5938.

Thornton, E. B., and R. T. Guza (1986), Surf zone longshore currents and random waves: Field data and models, *J. Phys. Oceanogr.*, *16*, 1165–1178.

Thornton, E. B., R. T. Humiston, and W. Birkemeier (1996), Bar-trough generation on a natural beach, *J. Geophys. Res.*, *101*, 12,097–12,110.

Trowbridge, J., and S. Elgar (2001), Turbulence measurements in the surf-zone, *J. Phys. Oceanogr.*, *31*, 2403–2417.

A. Apotsos, S. Elgar, and B. Raubenheimer, Woods Hole Oceanographic Institution, Woods Hole, MA 02543, USA. (aapotsos@whoi.edu)

R. T. Guza and J. A. Smith, Scripps Institution of Oceanography, 8602 La Jolla Shores Drive, La Jolla, CA 92037, USA.